Investigations of Rotation of Axial Ligands in Six-Coordinate Low-Spin Iron(III) Tetraphenylporphyrinates: Measurement of Rate Constants from Saturation Transfer Experiments and Comparison to Molecular Mechanics Calculations

Konstantin I. Momot and F. Ann Walker*

Department of Chemistry, University of Arizona, Tucson, Arizona 85721

Received: October 18, 1996; In Final Form: January 30, 1997[⊗]

Saturation transfer experiments have been utilized to measure the rate of axial ligand rotation in (tetramesitylporphyrinato)iron(III) bis(2-methylimidazole), $[(TMP)Fe(2\text{-}MeImH)_2]^+$. Saturation transfer peak intensities of four distinct pyrrole protons have been measured at a series of temperatures. Derivation of analytical expressions for steady-state peak intensities in the case of cyclic four-site exchange allowed the determination of the exchange rate constant. Previously measured longitudinal relaxation rate constants of the pyrrole protons of $[(TMP)Fe(2\text{-}MeImH)_2]^+$ have been used for rate constant determination. The temperature dependence of the rates has allowed estimation of the enthalpy barriers and entropy of this rotation. Modified MM2 potentials have also been used to study the rotation of axial ligands in $[(TMP)Fe(1,2\text{-}Me_2Im)_2]^+$ and (tetraphenylporphyrinato)iron(III) bis(1-methylimidazole), $[(TPP)Fe(1\text{-}MeIm)_2]^+$. The "adiabatic" potential energy surfaces (PES) for rotation of axial ligands (minima achieved in all degrees of freedom except for constrained internal rotation coordinates for the two axial ligands) have been constructed for both complexes by combining a Ramachadran-type dihedral drive with geometry minimization or Monte Carlo single minimum analysis with subsequent geometry minimization. The PES of the TMP-hindered imidazole complex indicates that the preferable mode of rotation is synchronous clockwise or counterclockwise rotation of the two axial ligands, with an enthalpy barrier to such rotation of approximately 48 kJ/mol. For the TPP-nonhindered imidazole complex, enthalpy barriers to synchronous and asynchronous rotation were found to be 3.3 and 5.4 kJ/mol, respectively, thus prompting the assumption that no particular mode of rotation is highly preferable in that complex. The rotational enthalpy barrier for the TMP-hindered imidazole complex was found to be consistent with experimental measurements of the current (59 kJ/mol) and previous work (50−54 kJ/mol) (Shokhirev, N. V.; Shokhireva, T. Kh.; Polam, J. R.; Watson, C. T.; Raffii, K.; Simonis, U.; Walker, F. A. *J. Phys. Chem. A* **1997**, *101*, 0000. Nakamura, M.; Groves, J. T. *Tetrahedron* **1988**, *44*, 3225). The relationship between the orientation of axial ligands, the distortion of the metalloporphyrin core from planarity, and the bulkiness of axial ligands and porphyrin substituents is discussed.

Introduction

Heme proteins possess a wide range of biochemical roles, which are defined by a large number of factors. Some of these factors are associated with the metal binding sites of the proteins, for which synthetic metalloporphyrin complexes have been shown to be promising models.[1] Three major variables in a model metalloporphyrin complex include the metal ion, the substituents on the porphyrin ring, and the type and number of axial ligands. These variables are also present in metal binding centers of heme proteins. In the heme proteins, axial ligands are provided by protein side chains, which can include those of histidine, methionine, cysteine, and other amino acids. They are constrained by covalent bonding to the protein backbone, coordination to the metal, and steric forces from the protein and are therefore kept in a definite orientation. The relative orientation of planar axial ligands has been shown to define EPR and NMR spectra of heme proteins and model hemes.[2−6] In model hemes, however, axial ligands appear to rotate freely and to adopt a variety of orientations with respect to each other and the porphyrin nitrogens. We[7−10] and others[11,12] have shown that modification of axial ligands and porphyrin substituents can allow one to control the orientation of axial ligands and the time scale of their rotation. Axial ligands and porphyrin substituents can also provide a certain degree of control of the general "shape" of the metalloporphyrin core, such as the type and the extent of its distortion from planarity. Previous studies indicate that orientation (and hence rotation) of axial ligands may be closely related to how much the porphyrin ring is distorted from planarity.[3,4,13] This suggests that studying orientation and rotation of axial ligands in model hemes can provide information about the shape of the metalloporphyrin core, which, in turn, can be an indication of how much the porphyrin ring may be distorted from planarity in an analogous heme protein.

In symmetric six-coordinate metallotetraphenylporphyrinate complexes with perpendicular orientation of unsymmetrical axial ligands such as 2-methylimidazole, rotation of axial ligands induces four-site exchange between pyrrole and between phenyl protons.[7] In low-spin iron(III) or cobalt(III) tetramesitylporphyrinate complexes, the peaks arising from distinct pyrrole and other protons close to the metal center are well-resolved from each other and other peaks,[7,8] which makes them ideal candidates for studying the rotation of axial ligands. In particular, in complexes with *ortho*-substituted phenyl rings and bulky axial ligands, rotation was found to be slow enough to be studied by NMR methods.[7,8,11,12] The temperature dependence of the rate of rotation of 2-methylimidazole ligands in (tetramesitylporphyrinato)iron(III) bis(2-methylimidazole), $[(TMP)Fe(2\text{-}MeImH)_2]^+$, and other related complexes has been measured from

[⊗] Abstract published in *Advance ACS Abstracts,* March 15, 1997.

S1089-5639(96)03235-5 CCC: $14.00

line shape changes of 1D NMR signals[11,12] and from peak intensities in 2D EXSY experiments.[8] In both cases, the value of the enthalpy of rotation was found to be in the vicinity of 50−54 kJ/mol. The entropy of rotation has also been measured in both studies and found to be small and positive, but the experimental error of the entropy measurement exceeds its absolute value. These parameters indicate that the rotation rate constant, k, ranges approximately from 0.5 to 50 s^{-1} in the temperature range −65 to −30 °C and can be accurately measured at any given temperature by the aforementioned NMR methods. In the current work, another approach for measuring the rate of axial ligand rotation is proposed, which is based on saturation transfer experiments. The basis for such an approach is that when one spin in an exchange pattern is irradiated, its longitudinal magnetization is transferred to other spins in the pattern. As a result, all spins in the pattern appear as absorption peaks whose relative intensities depend, along with other factors, on the rate of exchange. Although the mechanism of saturation transfer due to exchange is different from that for the NOE, the formal aspects of it are almost identical to the transfer of NOE in the extreme slow motion limit. Since NMR saturation transfer has first been introduced as a method of studying kinetic processes,[14] the method has been used extensively to study two-site[15−18] and more complex[19−21] exchange, as well as biochemical systems.[22−26] Although significant methodological developments[27,28] have occurred since its introduction, application of saturation transfer to complex exchange patterns is usually hindered by the complexity of the equations that arise, which can make interpretation of the results very difficult.[29] Difficulties can be avoided in some special cases, such as $k \gg R$. In the current work, the derivations and interpretation were facilitated by two factors. First, the cyclic four-site exchange between pyrrole protons has only one rate constant.[8] Second, relaxation rates of the four pyrrole protons, R, can be considered to be approximately the same. Although the second assumption potentially introduces some error in the interpretation, this approach can provide at least a good estimate of the rotational parameters. Knowledge of longitudinal relaxation rates of protons in the exchange pattern is needed for the determination of k. The values used in this work are taken from previous measurements from this laboratory.[30]

The results of the experimental rotation rate measurement have been interpreted in light of molecular mechanics studies of two model hemes, $[(TMP)Fe(1,2\text{-}Me_2Im)_2]^+$ and $[(TPP)Fe(1\text{-}MeIm)_2]^+$. Molecular mechanics and MM-based molecular dynamics methods have been used previously to study the dynamic behavior of protein metal binding sites and model hemes.[13,31,32] The biggest challenge in such studies seems to be finding appropriate molecular mechanics parameters, and most authors point out the importance of development of a potential for each specific system.[13,31,32] In this study, we used two MM potentials previously developed specifically for low-spin iron(III) porphyrinates.[13,32] Their adequacy and applicability limits will be discussed further below.

Molecular mechanics calculations in this work were intended to answer two questions. The first one is: What factors determine the mutual orientation of axial ligands in metalloporphyrin complexes, and what are the factors defining the rate of their rotation? The second question is whether molecular mechanics is an appropriate tool for the prediction of internal rotation barriers in such complexes and for the interpretation of NMR measurements. Below, we discuss the possible effects of the steric bulkiness of the complex on the orientation of its axial ligands and the rate of their rotation.

Experimental Section

Materials. Synthesis of iron(III) tetramesitylporphyrinates utilized for this study has been described elsewhere.[33] The 2-methylimidazole was purchased from Aldrich and used as received. A degassed sample of the bis(2-methylimidazolyl)-iron(III) tetramesitylporphyrinate complex with a slight excess of 2-MeImH was prepared in a 5 mm NMR tube in deuterated methylene chloride, CD_2Cl_2 (Cambridge Isotope Laboratories).

NMR Spectra. ^{1}H NMR spectra of $[(TMP)Fe(2\text{-}MeImH)_2]^+$ in the temperature range −40 to −70 °C were recorded on a Varian Unity-300 spectrometer operating at 299.955 MHz; spectra of $[(TPP)Fe(1\text{-}MeIm)_2]^+$ derivatives[30] were recorded on a Bruker AM500 spectrometer operating at 500.136 MHz. The variable temperature unit of the Unity-300 was calibrated using the Wilmad standard methanol sample. The temperature calibration curve was constructed by polynomial regression[34] using Matlab 4.1.1 for SGI workstations.[35] Saturation transfer spectra were recorded using a macro written locally. Typical experimental parameters were as follows: spectral bandwidth, 25 kHz; acquisition time, 0.196 s; number of points, 9792; number of transients, 196, plus four steady state transients before each new FID; irradiation time, 5 s; detection with 90° (typically 8 μs) pulse. Irradiation power was chosen so that only the target peak is irradiated. The irradiation bandwidth was controlled by irradiating a diamagnetic region with high peak density and adjusting the decoupler power so that the bandwidth is slightly smaller than the line width of the pyrrole proton signals. Additional control was provided by observing the peak intensities in recorded spectra. In cases when a peak next to the irradiated one is connected to the latter by a double jump, the intensity of such peaks should be not greater than the intensity of peaks connected by a single jump to the irradiated signal. Reference 1D spectra were recorded using the standard 1-pulse sequence with 16 transients and other parameters as described above, except for irradiation. Spectra were processed using Felix 2.30 for SGI workstations;[36] processing included zero filling to 8K complex points, exponential apodization to achieve the maximum apparent S/N ratio, Fourier transformation, phasing, and base line correction. Because of variations of S/N ratios and relative intensities of peaks with temperature, different base line correction procedures were used with different series of spectra. Spectra recorded at −47 and −56.5 °C were base line corrected using Wüthrich's base line flattening.[37] In spectra recorded at −37 and −67 °C, regions of 3000 complex points centered around the four pyrrole peaks were selected, and polynomial correction of third and fifth order, respectively, was applied to the selected regions. Peaks were integrated "to base line level". In each spectrum, two integration regions of similar width containing only noise were also integrated, and these integrals were used as error bars for peak intensities. For an alternative source of peak intensities, peak heights were measured by Felix' Peak Picking command. In measuring peak intensities, care has been taken to set the threshold so that only one peak is picked by the software for each "actual" pyrrole proton line. This measure is necessary because of the way Felix software determines the peak height in peak picking.[36] For each of the four pyrrole peaks irradiated, the value of the rate constant k was obtained as described in Data Analysis. Hence, four different measurements of k were obtained at each temperature for determination of the activation enthalpy and entropy of the exchange process (ligand rotation).

Calculations. Modifications of the MM2 potential for $[(TPP)Fe(1\text{-}MeIm)_2]^+$ were taken from a study by Munro et al., and a more recent modification[13] was used for [(TMP)Fe-

$(2\text{-MeImH})_2]^+$. Structural data for $[(TMP)Fe(1,2\text{-}Me_2Im)_2]^+$,[13] $[(TPP)Fe(1\text{-MeIm})_2]^+$,[38] and the free-base $TMPH_2$[39] were taken from the referenced sources. For $[(TPP)Fe(1\text{-MeIm})_2]^+$, the procedure for obtaining the adiabatic potential energy surface (PES) consisted of dihedral drive of the angle between the two axial ligands with a step of 30° throughout the 360° range and the dihedral drive of the angle of one of the two axial ligands in steps of 10° in the range 0−90°. For each dihedral drive step, conjugate gradient minimization with a loose convergence criterion and final full matrix Newton−Rafson minimization to gradient convergence below 0.01 kJ/(Å·×d7mol) were performed. All 130 (13 × 10) points of the PES for the TPP complex were obtained independently. For $[(TMP)Fe(2\text{-MeImH})_2]^+$, the procedure included a dihedral drive for each axial ligand with 20° step size, a single minimum Monte Carlo search, preminimization with a loose convergence criterion, and conjugate gradient minimization of the lowest energy preminimized structure to gradient convergence below 0.001 kJ/(Å·mol). When such gradient convergence could not be achieved, minimization was performed until no measurable change in energy could be observed. To perform the Monte Carlo search, both imidazole rings were opened at the N_1-C_5 bond and the porphyrin ring was opened at three different bonds near the *meso*-carbons. After that, five randomly selected torsion angles out of a possible ten angles were varied, and all rings previously open were closed again. The angles to be varied included one torsional angle (C_2-N_3) in each imidazole ring (varied by up to ±45°), two torsions around Fe−N bonds of the porphyrin core (up to ±45°), and all four $C_{meso}-C_{Ph}$ torsions (varied up to ±180°). A set of 1000 Monte Carlo steps was used for each pair of angles in the dihedral drive, each next step's structure being generated by random walk in the space of the varied torsion angles. For this PES, only 50 unique points were calculated using this procedure. The rest of the total of 361 (19 × 19) points were obtained from the unique points using the symmetry properties shown in Table 3 below.

In addition to the constructed adiabatic PES, the nonadiabatic barrier to collective rotation of perpendicularly oriented ligands in the TPP complex was estimated from constant-temperature molecular dynamics. All atoms in the molecule were given random velocities at the initial moment of time, which was followed by a 35 ps equilibration run (300 K; thermal bath constant, 0.067 ps). After equilibration, the molecule was allowed to evolve for 5 ns under the same thermodynamic parameters. During the 5 ns run, the values of the dihedral angle between the two axial ligands and angles between the two ligands and the porphyrin ring were recorded every 0.01 ps. The general procedure for the analysis of the output is described in Data Analysis. The resolution of the population map was 3° for each of the three angles monitored, and the total number of points in the map (and on the molecular dynamics trajectory) was 500 000. Axial ligands were considered "perpendicular" if the angle between them fell in one of the following ranges: +84° to +96° or −96° to −84°. Three separate MD runs with different initial conditions were performed; the nonadiabatic rotational barrier was estimated from each of them and then averaged. Calculations for $[(TMP)Fe(2\text{-MeImH})_2]^+$ were performed using Macromodel 4.5/BatchMin 4.5.[40] For $[(TPP)Fe(1\text{-MeIm})_2]^+$, calculations were performed using Macromodel 4.0/BatchMin 4.0.[41]

Data Analysis

NMR Data. Steady-state experiments involving transfer of longitudinal magnetization are described in the most concise form by the Solomon equations.[29] In addition to the term describing relaxation, exchange and irradiation terms have been added:

$$d\bar{\mathbf{M}}/dt = (\hat{\mathbf{K}} + \hat{\mathbf{S}})\bar{\mathbf{M}} + \hat{\mathbf{R}}(\bar{\mathbf{M}} - \bar{\mathbf{M}}_0) = 0 \qquad (1)$$

where

$$\hat{\mathbf{K}} = \begin{pmatrix} -2k & k & k & 0 \\ k & -2k & 0 & k \\ k & 0 & -2k & k \\ 0 & k & k & -2k \end{pmatrix} \qquad (2)$$

$$\hat{\mathbf{S}} = -\begin{pmatrix} S & 0 & 0 & 0 \\ 0 & 0 & 0 & 0 \\ 0 & 0 & 0 & 0 \\ 0 & 0 & 0 & 0 \end{pmatrix} \qquad (3)$$

$$\hat{\mathbf{R}}(\bar{\mathbf{M}} - \bar{\mathbf{M}}_0) = \begin{pmatrix} -R_{1A} & 0 & 0 & 0 \\ 0 & -R_{1B} & 0 & 0 \\ 0 & 0 & -R_{1C} & 0 \\ 0 & 0 & 0 & -R_{1D} \end{pmatrix} \begin{pmatrix} M_{zA} \\ M_{zB} \\ M_{zC} \\ M_{zD} \end{pmatrix} + \begin{pmatrix} R_{1A}I_{A\infty} \\ R_{1B}I_{B\infty} \\ R_{1C}I_{C\infty} \\ R_{1D}I_{D\infty} \end{pmatrix} \qquad (4)$$

The term describing the NOE was neglected, because our previous measurements[30] indicated that the rate of cross-relaxation is approximately 100 times smaller than the rate of longitudinal relaxation. No anomalous intensities were observed that could be attributed to the NOE. At temperatures where no exchange can be observed (*ca.* −90 °C), still no NOE could be detected in steady-state experiments. From these observations, it was concluded that the effect of the NOE on steady-state intensities of pyrrole protons is within the level of noise and therefore can be neglected without any significant bearing on the accuracy of interpretation of experimental measurements.

In eq 2, the 4 × 4 matrix describes cyclic four-site exchange between the pyrrole protons.[8] Equation 3 describes the situation where the first spin (hereafter referred to as spin *A*) is irradiated, *S* being the rate of irradiation-induced saturation of that peak. *S* depends on the irradiation intensity, but the exact form of the dependence is unknown. In eq 4, R_1 are longitudinal relaxation rates of appropriate protons, and I_∞ are their equilibrium longitudinal magnetizations. Arbitrary permutations of spins *A*−*D* can be made, as long as the matrices are modified accordingly. The following convention will be accepted throughout this paper, in accordance with eqs 2 and 3: *A* is the peak being irradiated, *B* and *C* are the peaks to which magnetization is transferred from *A* *via* a single jump, and *D* is the peak to which magnetization is transferred from *A* *via* a double jump (and from *B* and *C* *via* a single jump) (Figure 1, ref 8).

Setting each of eqs 1 to equal 0 designates a steady state and produces a system of nonhomogeneous linear equations that can be solved exactly using Kramer's rule.[42] Intensities of peaks in NOE difference spectra can be obtained by finding solutions for two cases, $S = 0$ and $S \neq 0$, and taking the difference of the two. Because *S* and I_∞ are unknown parameters, relative peak intensities in NOE difference spectra $\Delta A - \Delta D$ should be independent of *S* and I_∞ for the solution to be useful. This can be achieved by making the following two approximations:

$$R_{1A} = R_{1B} = R_{1C} = R_{1D} = R$$

$$I_{A\infty} = I_{B\infty} = I_{C\infty} = I_{D\infty} = I \qquad (5)$$

TABLE 1: Rate Constants for Exchange at Different Temperatures and Their Standard Errors

	rate measured from given peak, s^{-1}			
T, K	peak 1	peak 2	peak 3	peak 4
233.3	63 ± 6	52 ± 8	49 ± 3	47 ± 10
223.3	15 ± 2	14 ± 2	14 ± 1	13 ± 3
213.5	2.6 ± 0.4	2.7 ± 0.2	2.9 ± 0.7	2.4 ± 0.7
204.0	0.6 ± 0.1	0.5 ± 0.3	0.7 ± 0.1	0.7 ± 0.3

Under approximations (5), intensities of peaks in a saturation transfer spectrum are described by

$$\delta A/I_\infty = \xi(2k^2 + 4kR + R^2)$$

$$\Delta B/I_\infty = \Delta C/I_\infty = \xi(2k^2 + kR)$$

$$\Delta D/I_\infty = 2k^2\xi \tag{6}$$

where ξ is a parameter that depends on *S*, *k*, and *R*.

Once intensities $\Delta A-\Delta D$ and relaxation rate *R* are known, multiple methods can be used to extract *k*. The one chosen in this work was least squares fitting of experimental intensities to functions 6. Practically, this was accomplished using the "Curve Fitting" utility of SigmaPlot 5.0.[43] The relaxation rate *R* was taken as the average of the relaxation rates of the four pyrrole protons at the given temperature and was not varied during the least squares fit. Each intensity was fitted to its own function, *i.e.*, the irradiated peak to the function $\Delta A/I_\infty$, two direct (single-jump) exchange peaks to the function $\Delta B/I_\infty$, and the indirect (double-jump) exchange peak to the function $\Delta D/I_\infty$. The parameters varied in each fit were ξ and *k*. That is, four points were fitted to two parameters. Standard errors quoted for *k* in Table 1 were also calculated by the fitting utility.

It was assumed that variation of the exchange rate with temperature is consistent with activated complex theory. The values of $\Delta H^\ddagger$ and $\Delta S^\ddagger$ were determined using linear regression of $\ln(kh/k_BT)$ versus $1/T$. Standard errors for $\Delta H^\ddagger$ and $\Delta S^\ddagger$ were calculated in the linear regression procedure.[34]

Molecular Dynamics Data. Rotation of axial ligands in a metalloporphyrinate can be described in terms of a series of conformations, each of which is defined by three angles: the dihedral angle between the two axial ligands (α), the angle between an axial ligand and one of the four $Fe-N_{porph}$ bonds (β), and a similar angle for the second axial ligand (γ), in the first approximation only two of which are independent. The three angles can be monitored in a molecular dynamics run, so a series of points comprising a trajectory in conformational space of the three angles is generated. Each point is then mapped on a three-dimensional array describing populations of the conformational space. If map resolutions for the three angles are Δ_1, Δ_2, and Δ_3, then the point (α, β, γ) contributes to the map element

$$\left(\frac{\beta+180}{\Delta_1}+1, \frac{\beta+180}{\Delta_2}+1, \frac{\gamma+180}{\Delta_3}+1\right) \tag{7}$$

Distribution of angles β and γ while α is close to $\pm 90°$ can then be obtained as

$$n^\perp(\beta) = \sum_{\alpha=+90-\delta}^{+90+\delta}\sum_{\gamma=0}^{+360} m(\alpha,\beta,\delta) + \sum_{\alpha=-90-\delta}^{-90+\delta}\sum_{\gamma=0}^{+360} m(\alpha,\beta,\gamma) \tag{8}$$

$$n^\perp(\gamma) = \sum_{\alpha=+90-\delta}^{+90+\delta}\sum_{\beta=0}^{+360} m(\alpha,\beta,\gamma) + \sum_{\alpha=-90-\delta}^{-90+\delta}\sum_{\beta=0}^{+360} m(\alpha,\beta,\gamma) \tag{9}$$

Distributions 8 and 9 represent populations in a canonical ensemble of conformations generated by constant-temperature molecular dynamics. Population of states in a canonical ensemble is governed by the Boltzman distribution. Therefore the potential energy curve for collective rotation of perpendicular axial ligands can be obtained as[44]

$$E^\perp(\beta) = -RT\ln\left(\frac{n^\perp(\beta)}{\sum_{\beta=0}^{+360} n^\perp(\beta)}\right) \tag{10}$$

$$E^\perp(\gamma) = -RT\ln\left(\frac{n^\perp(\gamma)}{\sum_{\gamma=0}^{+360} n^\perp(\gamma)}\right) \tag{11}$$

Because angles β and γ are equivalent from the symmetry point of view, potential curves $E^\perp(\beta)$ and $E^\perp(\gamma)$ both have the same meaning. The fact that the origin for potential energy is arbitrary in (10) and (11) is irrelevant for barrier determination. The barrier can be obtained as the difference between the maximum and the minimum values of *E* from both potential energy curves and averaged.

Results and Discussion

With respect to rotational behavior of axial ligands, $[(TMP)Fe(2\text{-}MeImH)_2]^+$ and $[(TPP)Fe(1\text{-}MeIm)_2]^+$ represent two extremes. $[(TMP)Fe(2\text{-}MeImH)_2]^+$ exhibits axial ligand rotation that can be considered slow on the NMR time scale ($k \sim 1-100$ s^{-1}). This complex has a well-defined equilibrium orientation of axial ligands; their rotation is extremely hindered and does not lead to averaging of pyrrole proton signals or even dramatic changes in their line widths below −35 °C. Slowly rotating axial ligands in $[(TMP)Fe(2\text{-}MeImH)_2]^+$ are the source of inequivalence of the four pyrrole protons. Their rotation induces exchange between pyrrole protons (Figure 1, ref 8), and the pattern of the exchange is consistent with axial ligands rotating slowly while maintaining perpendicular orientation with respect to each other.

On the other hand, rotation of axial ligands in $[(TPP)Fe(1\text{-}MeIm)_2]^+$ is extremely fast on the NMR time scale. Because it is fast, only the lower estimate for the rate of exchange can be obtained. For convenience we will assume that for unsubstituted TPP complexes the typical distance between inequivalent pyrrole signals would be similar to that for the TMP complex of this study, or of the order of 5 ppm, which corresponds to 2500 Hz at a 500 MHz field. For exchange to be fast, the rate of exchange has to be much larger than $2\pi(\Delta\nu)$. Hence, the lower estimate of 2×10^4 s^{-1} can be obtained for the rate of exchange in $[(TPP)Fe(1\text{-}MeIm)_2]^+$ from the fact that the 1D proton NMR spectrum shows a single peak at 500 MHz. The $(1\text{-}MeIm)_2$ complexes of all symmetrical iron(III) tetraphenylporphyrinates studied to date, including the TMP complex,[45] exhibit only one pyrrole signal down to −90 °C, which is consistent with the assumption that any inequivalence caused by axial ligands is averaged by their fast rotation. That *ortho*-substituted TPP complexes are unique in having slow ligand rotation is also shown by the fact that $[(TPP)Fe(2\text{-}MeImH)_2]^+$ has only one resolved pyrrole-H resonance, which only begins to broaden below −80 °C and does not reach the slow exchange regime until somewhere below −95 °C.

From the above discussion, it should be clear that NMR methods can only be useful for measuring the rate of exchange in $[(TMP)Fe(2\text{-}MeImH)_2]^+$, but not in $[(TPP)Fe(1\text{-}MeIm)_2]^+$.

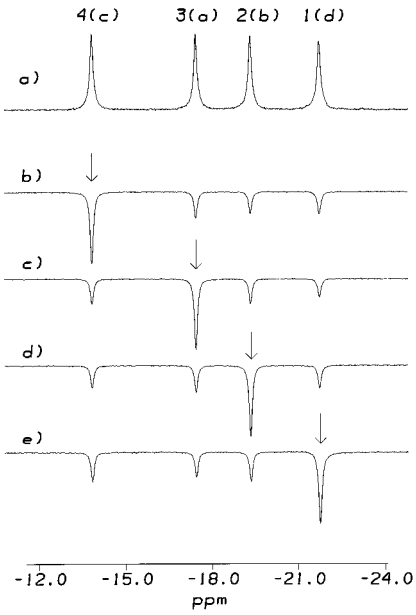

Figure 1. (a) 1D ^{1}H NMR spectrum of the pyrrole-H region of [(TMP)-Fe(1-MeImH)$_2$]$^+$ in CD_2Cl_2 at 226 K; (b−e) examples of saturation transfer difference spectra for the same complex at the same temperature, irradiation time 5 s, obtained by subtracting spectra with target peaks irradiated from the reference spectrum (irradiation of an "empty" region downfield from all peaks). Only the pyrrole region is shown, because although NOESY/EXSY spectra clearly show NOE cross-peaks as well as peaks arising from chemical exchange of pyrrole-H, *o*-CH_3, *m*-H, and *p*-H resonances of this complex,[8] no saturation transfer peaks arising from NOE were observed in the present work.

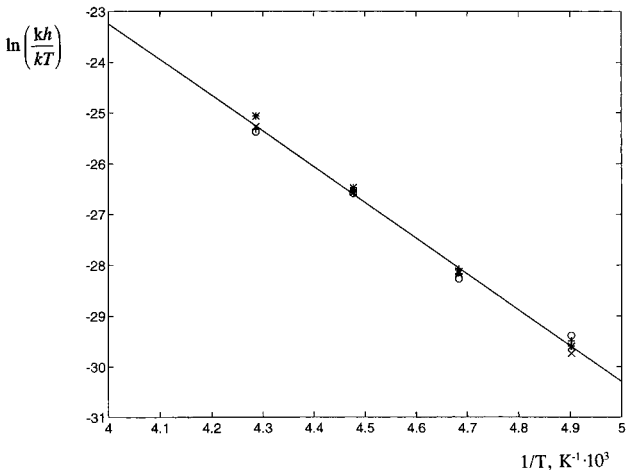

Figure 2. Fitting of experimentally determined rate constants to obtain thermodynamic activation parameters: *, peak 1; ×, peak 2; +, peak 3; ○, peak 4.

In the accompanying work,[8] phase-sensitive EXSY spectra were used to measure the rate of exchange. These results are included in Table 2, to be presented below. In the present work, saturation transfer spectra recorded at large irradiation times are proposed as an alternative and possibly faster way to estimate the exchange rate constant. Examples of the spectra obtained are shown in Figure 1. Table 1 and Figure 2 summarize the results of all measurements at four different temperatures. A generally good agreement between different measurements within each temperature series is evident. We could not establish any definite trends in discrepancies between different measurements, such as irradiation of one particular peak yielding consistently overestimated or underestimated values of the rate constant. It is possible (although not very likely, as discussed below) that the discrepancies are primarily due to random

TABLE 2: Thermodynamic Parameters for Exchange in TMP Complexes from Various Measurements

method	$\Delta H^‡$, kJ/mol	std err	$\Delta S^‡$, J/(K·mol)	std err
NMR (saturation transfer)[a,b]	59	1	41	5
NMR (EXSY)[b,c]	51	3	3	15
NMR (DNMR line shape)[b,d]	54	2	16	7
current MM2[a,e]	48	not measured		

[a] This work. [b] [(TMP)Fe(2-MeImH)$_2$]$^+$. [c] Reference 8. [d] Reference 11. [e] [(TMP)Fe(1,2-Me$_2$Im)$_2$]$^+$.

residual deficiencies in the base line of the experimental spectra. We have found that the least squares fitted value of the rate constant is sensitive to the base line correction, especially in cases where the peak intensities are very close to each other (−40 °C) or nonirradiated peaks have much lower intensity than the irradiated one (−70 °C). With that in mind, we have chosen methods of base line correction for each temperature series so that the correction would give the same quality and the best possible base line for all spectra of each series.

Along with poor base line correction as a possible source of error, two systematic sources can be named. The first is different T_1 relaxation times for the four different pyrrole signals. The formalism described in "NMR Data Analysis" uses the assumption that relaxation rates for all four pyrrole protons are the same. However, the actual relaxation rates can differ by as much as 20%, especially for pyrrole signal 1 (proton *d*), which at all temperatures exhibits a somewhat shorter T_1 than the three other pyrrole protons. Unfortunately, we were not able to find a way to avoid using this assumption, because to do so would require the knowledge of the rate of irradiation-induced transitions (parameter ***S***). The second potential source of systematic error is present when not long enough irradiation time is used in the saturation transfer experiments, and a steady state is not established. We believe that this source of error was avoided in this work, because the time used (5 s) is much longer than the characteristic time of any magnetization relaxation process involved, as well as because the use of irradiation time of 10 s yields spectra with essentially identical relative peak intensities.

In Table 2, Eyring activation parameters for exchange determined from the saturation transfer measurements are presented and are compared to literature values determined by other NMR techniques. Two distinctions from previous NMR measurements can be seen. First, the exchange enthalpy measured from saturation transfer is roughly 10−15% larger than the values obtained from other NMR techniques. Second, the entropy of exchange is significant compared both to the standard error of least squares fitting and to the results of the measurements by other methods. The lower confidence level for the activation entropy, defined as the expectation value of the entropy from which the standard deviation of the entropy value has been subtracted, is noticeably higher than the expectation values of the entropy obtained from other methods in Table 2.

Three factors have been ruled out by us as possible sources of the difference. The first factor is a possible error in the determination of temperature. The variable-temperature unit of the spectrometer has been calibrated with the accuracy of 0.5 K or better. The temperature of the TMP complex sample was maintained with the same accuracy. Therefore, the combined error in temperature determination could not have exceeded 1 K. We have taken special care to avoid temperature-proportional error in the temperature measurement, when the error in the high-temperature range is positive, while the error in the low-temperature range is negative, or vice versa. Such temperature-proportional error leads to the largest error in the

TABLE 3: Symmetry Properties Used in Construction of Adiabatic PES of [(TMP)Fe(1,2-Me_2Im)$_2$]$^+$

ligand permutation rules	rotation rules	boundary conditions
$E(\alpha,\beta) = E(\beta,\alpha)$	$E(\alpha,\beta) = E(\alpha + 180,\beta \pm 180)$	$E(\alpha,0) = E(\alpha,360)$
$E(\alpha,\beta) = E(\beta \pm 180,\alpha \pm 180)$	$E(\alpha,\beta) = E(-\alpha,-\beta)$	$E(0,\beta) = E(360,\beta)$
$E(\alpha,\beta) = E(-\beta,-\alpha)$	$E(\alpha,\beta) = E(180-\alpha,180-\beta)$	
$E(\alpha,\beta) = E(180-\beta,180-\alpha)$	$E(\alpha,0) = E(-\alpha,0)$	
	$E(0,\beta) = E(0,-\beta)$	

[a] α and β are angles between two axial ligands and an arbitrary porphyrin ring nitrogen, as defined in "Data Analysis: Molecular Dynamics Data". Not all rules are independent.

determination of thermodynamic parameters of rotation. We also used the positions of pyrrole proton peaks as an alternative source of temperature calibration. Temperature calibration using the positions of pyrrole peaks was performed by the least squares fit of pyrrole positions to the previously determined dependencies of their positions as functions of temperature.[3,30] The use of such alternative temperature calibration yields the following activation parameters: $\Delta H^{\ddagger} = 55.2 \pm 1.2$ kJ/mol; $\Delta S^{\ddagger} = 28.8 \pm 5.5$ J/(K·mol). These ranges for $\Delta H^{\ddagger}$ and $\Delta S^{\ddagger}$ are shifted from our saturation transfer results shown in Table 2 toward lower $\Delta H^{\ddagger}$ and lower $\Delta S^{\ddagger}$. The two sets of ranges do not overlap, but those from the alternative source of the temperature calibration exhibit the same trend relative to the results of previous measurements: both sets show higher $\Delta H^{\ddagger}$ and higher $\Delta S^{\ddagger}$ than other methods.[8,11,12]

The second factor that has been ruled out as a possible source of the discrepancy is equilibrium between the complexed and the free forms of 2-methylimidazole that can lead to reorientation of the axial ligands and is therefore an additional source of exchange between pyrrole protons. We have two reasons to believe that dissociation of the ligands from the complex is not a factor affecting the results of our measurements. Firstly, discarding the points corresponding to the highest temperature (where the dissociation should be the most prominent) does not significantly change the activation parameters. The values of $\Delta H^{\ddagger}$ and $\Delta S^{\ddagger}$ obtained from the three lowest temperatures are 58.7 ± 1.8 kJ/mol and 41.6 ± 8.3 J/(K·mol), respectively. Secondly, the exchange parameters from the companion work[8] were obtained from an exchange study in the temperature range of −31 to −61 °C, which is higher than the temperature range studied in this work. However, the data obtained in the companion study[8] yield a near-zero $\Delta S^{\ddagger}$ and a smaller $\Delta H^{\ddagger}$.

Finally, the third possible source of error that has been deemed unlikely is serious base line imperfections leading to large error in peak intensities. Using peak heights (which are not as sensitive to the base line correction method) instead of integrals produces $\Delta H^{\ddagger} = 60 \pm 1$ kJ/mol and $\Delta S^{\ddagger} = 48 \pm 5$ J/(K·mol—that is, both parameters are still higher than those obtained in previous studies.

In light of the previous discussion it should be noted that the standard error for activation parameters given in Table 2 is the standard error of the linear regression procedure and does not reflect the error in peak intensity or rate constant (Table 1) determination. It is not clear to us at this time what is the exact cause of the difference from previous measurements. It is possible that the cause is in the interproton saturation transfer technique itself, or in the assumptions made in the determination of exchange rate constants, rather than any technical drawbacks in the experiment. However, we should mention that the consistency of different measurements made at the same temperatures is better in the current study than in the companion work,[8] and the correlation of our linear regression from which the thermodynamic parameters were obtained is also better.

Regardless of which set of the thermodynamic values is the "right" one, the saturation-transfer experiment can be used at least to estimate exchange activation parameters. The best accuracy of the method should be expected in the "intermediately slow" exchange mode—that is, when $I_A \gg I_B$, $I_C \gg I_D \gg I_{noise}$.

The conclusions reached from ^{1}H NMR spectra, both those of this work and those of refs 8, 11, and 12, are corroborated by molecular mechanics computations. Adiabatic potential energy surfaces in this work are constructed from the lowest energy points available for every orientation of the axial ligands. The term "adiabatic" in this case means that rotation is slow enough for the porphyrin core to adjust to every new orientation of the axial ligands. Intuitively, the characteristic time required for such adjustment should be comparable or smaller than several times the characteristic time of the lowest-frequency vibration of the porphyrin core. While hindered rotation of axial ligands in the TMP complex definitely meets such criteria, it can be questioned whether rotation in the TPP complex can actually be considered slow. However, data to be discussed below will demonstrate that adiabatic PES calculation is an acceptable way to at least roughly estimate the rotational $\Delta H^{\ddagger}$ in [(TPP)Fe(1−MeIm)$_2$]$^+$.

In the computational part of this work, [(TMP)Fe(1,2-Me_2Im)$_2$]$^+$ has been modeled rather than [(TMP)Fe(2-MeImH)$_2$]$^+$, which was used in NMR experiments. Comparison of calculated global minima for the two complexes shows that methyl groups in position 1 of the imidazole ligands have practically no effect on the equilibrium geometry when 2-methyl groups are present. DNMR measurements of activation parameters for the two complexes[11] also produce almost identical results (for the 1,2-Me_2Im complex, $\Delta H^{\ddagger} = 53 \pm 3$ kJ/mol and $\Delta S^{\ddagger} = 22 \pm 15$ J/(K·mol); for the 2-MeImH complex, 54 ± 2 kJ/mol and 16 ± 7 J/(K·mol), respectively).

The PES for the modeled TMP complex is shown in Figure 3b and exhibits several equivalent minima, all of them corresponding to perpendicular axial ligands bisecting the porphyrin nitrogens. All conformations with parallel axial ligands are either maxima or saddle points on the PES. The energy difference between lowest conformations with "perpendicular" and "parallel" axial ligands is 57 kJ/mol. This energy difference makes perpendicularly orientated axial ligands lying over *meso*-carbon positions of the porphyrin the preferred conformation. The PES also indicates that two modes of rotation of the axial ligands are potentially possible. The first mode involves both ligands rotating in the same direction while retaining their perpendicular orientation. The enthalpy barrier to such rotation is 48 kJ/mol. The second mode involves the axial ligands rotating in opposite directions and switching their relative orientation from +90° to −90°. The enthalpy barrier to this mode of rotation is 69 kJ/mol. At room temperature, the ratio of the rates of rotation corresponding to the two modes would be 4800:1, which makes us believe that contributions to the exchange pattern from the antisynchronous rotation are negligible. It should be noted that no entropy of rotation is measured in MM calculations; therefore the rates derived from computational results should be considered as order-of-magnitude estimates. However, it was demonstrated from the NMR experimental data presented above (Table 2) that the rotational

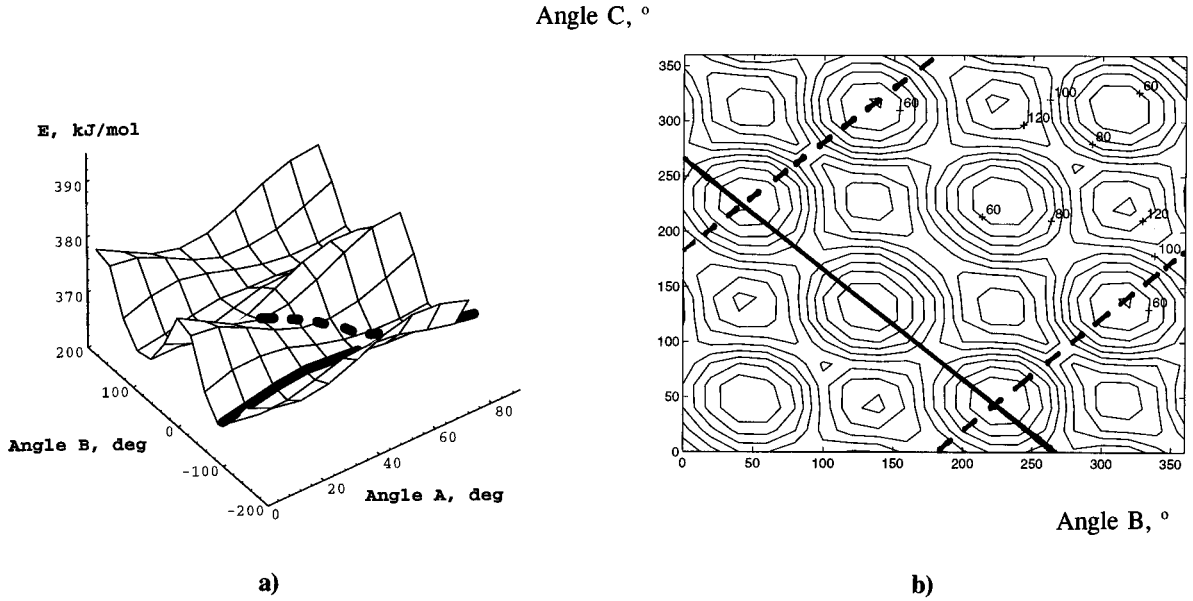

Figure 3. Adiabatic PES of axial ligand rotation for (a) $[(TPP)Fe(N-MeIm)_2]^+$ and (b) $[(TMP)Fe(1,2\text{-}Me_2Im)_2]^+$. Angle *A* is the dihedral angle between the planes of the two imidazole ligands, and angles *B* and *C* are the angles between the planes of the imidazole ligands and an arbitrarily chosen (but the same for both angles) $Fe-N_{porph}$ bond. The solid line on each plot shows a rotation path with the lower barrier (axial ligands rotate in the same direction), and the dashed line shows the rotation path that has the higher barrier (axial ligands rotate in the opposite directions). A set of two paths of rotation exists for each type of rotation (clockwise and counterclockwise), but only one path is shown in each case. The contour levels on plot b) are marked in kJ/mol; the distance between isolines is 10 kJ/mol.

TABLE 4: Calculated Activation Enthalpies of Different Modes of Axial Ligand Rotation in $[(TMP)Fe(1,2\text{-}Me_2Im)_2]^+$ and $[(TPP)Fe(1\text{-}MeIm)_2]^+$

	ΔH, kJ/mol	
	synchronous	antisynchronous
TMP	48	69
TPP	3.3	5.4

$\Delta S^{\ddagger}$ is probably small and is thus unlikely to affect the relative importance of different modes of rotation.

The adiabatic PES for $[(TPP)Fe(1\text{-}MeIm)_2]^+$ is shown in Figure 3a. As has been mentioned before, it is potentially less reliable for the determination of the $\Delta H^{\ddagger}$ of internal rotation of axial ligands. However, the results presented in Figure 4 show that it does give at least a rough estimate of the rotational energy. Figure 4 shows a distribution of values of the angle between one of the axial ligands and one of the $Fe-N_{porph}$ bonds (angle β), while the angle between the two axial ligands (angle α) is kept close to $\pm 90°$. This distribution reflects the population of conformations along the coordinate of synchronous rotation. Analysis of the population of conformations described in the section "Data Analysis: Molecular Dynamics Data" produces the energy of synchronous rotation of 4.5 ± 0.3 kJ/mol at 300 K, which, in turn, yields the rate of rotation on the order of magnitude of 10^{12} s^{-1}, a rate that is extremely fast on the NMR time scale. The presence of an activation entropy of rotation is likely to change this value by not more than 2 or 3 orders of magnitude, on the basis of the typical $\Delta S^{\ddagger}$ values obtained for different complexes.[8] Because both rotation channels in this case are fast, no experimental evidence from NMR data could be obtained regarding the exchange pattern. On the other hand, because complete rotational averaging is present, this information is irrelevant to the interpretation of NMR spectra of $[(TPP)FeL_2]^+$ complexes.

This qualitative agreement between results from NMR experiments and molecular mechanics calculations renders the latter a potentially useful and adequate tool for studying rotation of axial ligands. In addition to looking at the values of the

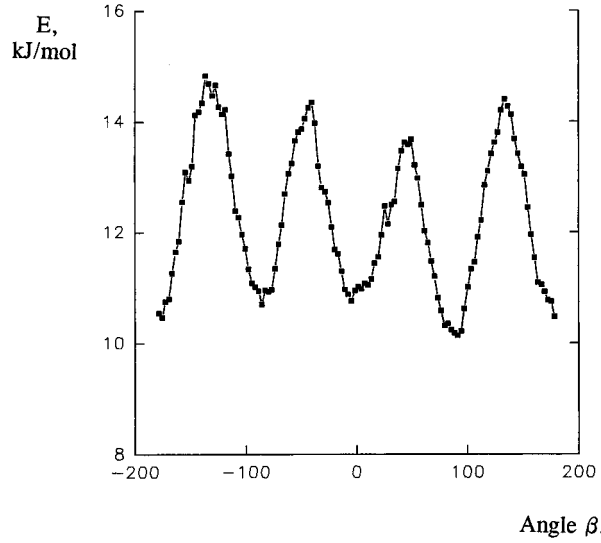

Figure 4. Example of a potential energy curve for collective rotation of perpendicular axial ligands obtained from Boltzman population analysis of the molecular dynamics output.

rates of rotation, it is also advantageous to consider the behavior of the metalloporphyrin core in the two "extreme" complexes. Crystal structures of the two complexes,[13,38] as well as calculated global minimum geometries shown in Figure 5, demonstrate that the TMP complex experiences very strong ruffling of its metalloporphyrin ring, while the ring in the TPP complex exhibits just a slight saddle-type distortion. On the other hand, the free-base tetramesitylporphyrin, $TMPH_2$,[39] experiences practically no distortion from planarity despite its bulky mesityl substituents. This suggests that the strong ring ruffling in the $[(TMP)Fe(2\text{-}MeImH)_2]^+$ complex is a result of strong steric interaction between bulky axial ligands and bulky substituents of the porphyrin ring. A similar conclusion has been reached in a previously published work by Munro *et al.*[13] Omitting electronic factors, one can say that lack of space to accommodate the axial ligands causes the porphyrin ring to distort from

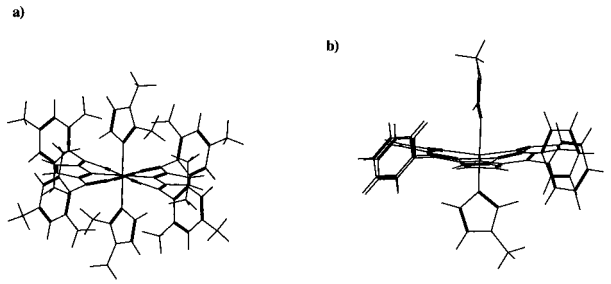

Figure 5. Global minimum geometries for (a) $[(TMP)Fe(1,2\text{-}Me_2Im)_2]^+$ and (b) $[(TPP)Fe(N-MeIm)_2]^+$. The geometry of the TMP complex is practically identical to the crystal structure of **(1)**, while orientation of axial ligands in the TPP complex does not reproduce that in the crystal structure.

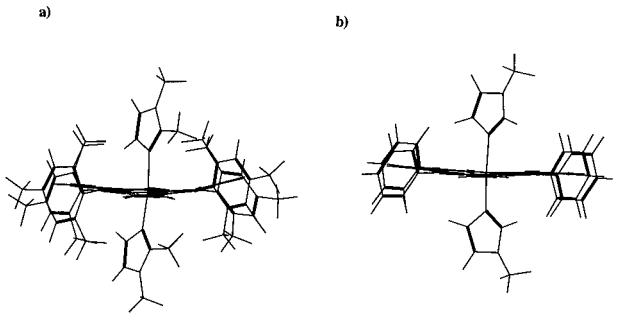

Figure 6. Geometries obtained from minimization of (a) $[(TMP)Fe(1,2\text{-}Me_2Im)_2]^+$ and (b) $[(TPP)Fe(N-MeIm)_2]^+$ when the orientation of both axial ligands is constrained and the ligands are parallel to each other. Note that in both cases the porphyrin ring's distortion from planarity is much smaller than in the global minima structures, where axial ligands are near-perpendicular.

planarity, which, in turn, makes perpendicular orientation of axial ligands even more favorable. It is probably not possible to say that one factor is the primary cause of the other; rather, it is a cooperative phenomenon where the orientation of axial ligands and the shape of the metalloporphyrin core are mutually dependent on each other. This hypothesis suggests that S_4-ruffling will be the predominant type of distortion when ligands bisect the porphyrin nitrogens, while D_{2d} saddle-type distortion will be more important when ligands eclipse the porphyrin nitrogens. Figure 6 illustrates that the ring is more likely to retain its planarity when axial ligands are forced to be in parallel planes. It should be noted that the PES calculated in this work do not take into account the energy of stabilization of low-spin d^5 systems that arises from the Jahn−Teller distortion, which favors parallel orientation of axial ligand planes, in the absence of steric factors.[2,3]

Further, examination of the two complexes in terms of the steric bulkiness of axial ligands and porphyrin ring substituents prompts the hypothesis that the rate of rotation and degree of distortion of the metalloporphyrin ring from planarity are related. The rationale for such a hypothesis is that, for axial ligands to successfully rotate, the ring has to assume planar conformation to allow the ligands to pass over the $Fe-N_{porph}$ bonds and then has to change the direction of its distortion by 90°. Our calculations show that the barrier to rotation over a metalloporphyrin ring that is frozen in one equilibrium conformation exceeds 115 kJ/mol even for $[(TPP)Fe(1\text{-}MeIm)_2]^+$; hence, the rate of rotation over a frozen ring would be by several orders of magnitude smaller than the rate of adiabatic rotation. This rationale should be especially true for complexes with bulky ligands and substituents. On the other hand, in complexes with bulky ligands and substituents the porphyrinate ring's distortion from planarity is larger; therefore the ring has to undergo larger

TABLE 5: Distortion of Metalloporphyrin Core from Planarity in $[(TMP)Fe(1,2\text{-}Me_2Im)_2]^+$ and $[(TPP)Fe(1\text{-}MeIm)_2]^+$

	ruffling, deg	saddle distance, Å	rate of exchange, s^{-1}	ligand−core distance, Å
TMP cr	43.3	0.001	∼50	2.816
TPP cr	5.4	0.025	$\gg 2 \times 10^4$	3.332
TMP calc	37.9	0.003		2.592
TPP calc	4.4	0.250		3.333

adjustments of its conformation for the rotation to occur. Data presented in Table 5 make an attempt to quantify distortions from planarity in the two complexes studied and to establish a relationship between distortions, bulkiness of substituents, and the rate of rotation. Two types of core distortions are usually distinguished in metalloporphyrinates, S_4 ruffling and D_{2d} saddle-type distortion.[32] S_4 ruffling is characterized by a tilt between two opposite pyrrole rings; the average dihedral angle between two pairs of pyrrole rings is used as a measure of ruffling in Table 5. D_{2d} saddle-type distortion is characterized by elevation of one pair of opposite pyrrole nitrogens and depression of the other pair with respect to the least-squares fit plane drawn through the four nitrogens and the metal. The extent of saddle-type distortion in Table 5 is calculated in the following way. Distances between four porphyrin nitrogens and the least squares fitted plane are calculated. The distances have a sign; in the case of a pure saddle distortion the distances for a pair of opposite nitrogens will have the same sign, and the signs will be different for the two pairs. The sums over the two pairs are subtracted from each other, and the difference is divided by 4 and taken as the absolute value.

The two complexes studied in this work cannot be considered a representative set for drawing any definitive conclusions about the relationship between the rate of rotation and the extent of distortion of the metalloporphyrin core from planarity. Other studies[3−5,45] have indicated that even the presence of a strong ruffling may not result in a rate of rotation that is slow on the NMR time scale. Such a relationship probably does not have the nature of a direct correlation, as evidenced by nearly equal rotation barriers for 2,6-Br_2- and 2,6-C_2-TPP complexes.[8] However, the general trend (that a lower distortion of the metalloporphyrin core from planarity results in a greater rate of axial ligand rotation) is evident even at this time. Ruffling and the rate of rotation are also correlated to the steric demands of axial ligands; five-membered ring imidazoles require less distortion of the porphyrin core and rotate faster than six-membered ring pyridines, which in turn rotate faster than "hindered" imidazoles such as 2-MeImH.[45]

It should also be noted that the experimental and calculated equilibrium geometries of the TPP complex are not the same. While in the crystal structure axial ligands are antiparallel and bisect the porphyrin nitrogens,[38] in the calculated structure they are nearly perpendicular ($\alpha = 103°$) and point roughly toward the porphyrin nitrogens. Also, the calculated structure has a larger degree of saddle-type distortion, probably a consequence of the perpendicular orientation of the axial ligands. The cause of the difference in ligand orientation is probably the fact that the MM2 force fields do not directly include factors related to the molecular orbital effects and Jahn−Teller distortion. Our calculations also did not include either crystal packing or solvent effects which can be present in the condensed phase. These factors should be a precaution against "literal" interpretation of the computational results, at least for the TPP complex where rotation is probably nonadiabatic. The fact that the calculated distortion from planarity is greater than that actually observed in the crystal structure suggests that the calculated exchange

energy barrier is more likely to overestimate the actual value rather than underestimate it—that is, rotation in $[(TPP)Fe(1\text{-}MeIm)_2]^+$ may be even faster than the molecular mechanics estimate.

It is evident to us that at least in the case of slow rotation steric interaction between the axial ligands and the metalloporphyrin core is the major factor determining the ligands' orientation and the rate of rotation. For the case of fast rotation, when the magnitude of the steric interaction is smaller, consideration of electronic effects is probably necessary. Crystal packing and solvent effects may also be important in the latter case.

We believe that this work demonstrates the great utility of molecular mechanics calculations for semiquantitative estimation of the rate of axial ligand rotation in bis-ligated metalloporphyrin complexes. While such calculations do not account for crystal packing, solvent, and possible Jahn−Teller effects and do not explicitly consider molecular orbital effects, they accurately describe the steric interaction of the axial ligands and the metalloporphyrin core. In cases when steric interaction is large and is the major factor determining the rotational barrier, molecular mechanics is expected to be an adequate tool for predicting the orientation and the rate of rotation of axial ligands. At least some of such cases will exhibit ligand rotation slow enough to be studied by NMR methods, enabling researchers to compare the results obtained from two independent sources. Further refinement of molecular mechanics potentials could be achieved by developing a pseudopotential describing overlap energy between the axial ligands' π-MOs and the metal atom's d-AOs and incorporating it into the force field. That should expand the applicability region to complexes with lower rotational barrier. Nonadiabatic ligand rotation in such cases could be dealt with by introducing a third PES coordinate corresponding to the extent of the porphyrin ring's out-of-plane distortion, although that would greatly increase the computational demands.

Acknowledgment. The support of this work by the National Institutes of Health, Grant DK 31038 (F.A.W.), the Materials Characterization Program at the University of Arizona, the Department of Chemistry for a Mid-Career Scholarship (K.I.M.), and the National Science Foundation, Grant CHE-9214383 (for purchase of the Varian Unity-300 NMR spectrometer), is gratefully acknowledged. We would also like to thank the reviewers for helpful comments. The authors are grateful to Dr. Nikolai Shokhirev for his invaluable discussions.

References and Notes

(1) Walker, F. A.; Simonis, U. Iron-Porphyrin Chemistry. In *Encyclopedia of Inorganic Chemistry*; King, R. B., Ed.; Wiley: Chichester, U.K., 1994; Vol. 4, pp 1785−1846.

(2) Walker, F. A.; Huynh, B. H.; Scheidt, W. R.; Osvath, S. R. *J. Am. Chem. Soc.* **1986**, *108*, 5288.

(3) Safo, M. K.; Gupta, G. P.; Walker, F. A.; Scheidt, W. R., *J. Am. Chem. Soc.* **1991**, *113*, 5497.

(4) Safo, M. K.; Gupta, G. P.; Watson, C. T.; Simonis, U.; Walker, F. A.; Scheidt, W. R. *J. Am. Chem. Soc.* **1992**, *114*, 7066.

(5) Safo, M. K.; Walker, F. A.; Raitsimring, A. M.; Walters, W. P.; Dolata, D. P.; Debrunner, P. G.; Scheidt, W. R., *J. Am. Chem. Soc.* **1994**, *116*, 7760.

(6) Shokhirev, N. V.; Walker, F. A. *J. Phys. Chem.* **1995**, *99*, 17795.

(7) Walker, F. A.; Simonis, U. *J. Am. Chem. Soc.* **1991**, *113*, 8652.

(8) Shokhirev, N. V.; Shokhireva, T. Kh.; Polam, J. R.; Watson, C. T.; Raffii, K.; Simonis, U.; Walker, F. A. *J. Phys. Chem. A* **1997**, *101*, 2778.

(9) Basu, P.; Shokhirev, N. V.; Enemark, J. H.; Walker, F. A. *J. Am. Chem. Soc.* **1995**, *117*, 9042.

(10) Basu, P.; Raitsimring, A. M.; Enemark, J. H.; Walker, F. A. *Inorg. Chem.*, in press.

(11) Nakamura, M.; Groves, J. T. *Tetrahedron* **1988**, *44*, 3225.

(12) Nakamura, M.; Tajima, K.; Tada, K.; Ishizu, K.; Nakamura, N. *Inorg. Chim. Acta* **1994**, *224*, 113.

(13) Munro, O. Q.; Marques, H. M.; Debrunner, P. G.; Mohanrao, K.; Scheidt, W. R. *J. Am. Chem. Soc.* 1995, *117*, 935.

(14) (a) Forsén, S.; Hoffman, R. A. *J. Chem. Phys.* **1963**, *39*, 2892. (b) Forsén, S.; Hoffman, R. A. *J. Chem. Phys.* **1964**, *40*, 1189.

(15) Caravatti, P.; Levitt, M. H.; Ernst, R. R. *J. Magn. Reson.* **1986**, *68*, 323.

(16) Knight, C. T. G.; Merbach, A. E. *J. Am. Chem. Soc.* **1984**, *106*, 804.

(17) Borzo, M.; Maciel, G. E. *J. Magn. Reson.* **1981**, *43*, 175.

(18) Saunders, J. K.; Bell, R. A. *Can. J. Chem.* **1970**, *48*, 512.

(19) Grassi, M.; Mann, B. E.; Pickup, B. T.; Spencer, C. M. *J. Magn. Reson.* **1986**, *69*, 92.

(20) Ugurbil, K. *J. Magn. Reson.* **1985**, *64*, 207.

(21) Perrin, C. L.; Johnston, E. R. *J. Magn. Reson.* **1979**, *33*, 619.

(22) Thanabal, V.; de Ropp, J. S.; La Mar, G. N. *J. Am. Chem. Soc.* **1987**, *109*, 265.

(23) Andersen, N. H.; Nguyen, K. T.; Eaton, H. L. *J. Magn. Reson.* **1985**, *63*, 365.

(24) Alger, J. R.; Shulman, R. G. *Q. Rev. Biophys.* **1984**, *17*, 83.

(25) Clore, G. M.; Gronenborn, A. M. *J. Magn. Reson.* **1983**, *53*, 423.

(26) Krishna, N. R.; Huang, D. H.; Glickson, J. D.; Rowan, R.; Walter, R. *Biophys. J.* **1979**, *26*, 345.

(27) Gesmar, H.; Led, J. J. *J. Magn. Reson.* **1986**, *68*, 95.

(28) Led, J. J.; Gesmar, H. *J. Magn. Reson.* **1982**, *49*, 444.

(29) Neuhaus, D.; Williamson, M. P. *The Nuclear Overhauser Effect in Structural and Conformational Analysis*; VCH: Weinheim, Germany, 1989; Chapter 5, and references cited therein.

(30) Momot, K. I.; Walker, F. A. Manuscript in preparation.

(31) (a) Hancock, R. D.; Weaving, J. S.; Marques, H. M. *J. Chem. Soc., Chem. Commun.* **1989**, 1176. (b) Lopez, M. A.; Kollman, P. A. *J. Am. Chem. Soc.* **1989**, *111*, 6212. (c) Thompson, M. A.; Schenter, G. K. *J. Phys. Chem.* **1995**, *99*, 6374.

(32) Munro, O. Q.; Bradley, J. C.; Hancock, R. D.; Marques, H. M.; Marsicano, F.; Wade, P. W. *J. Am. Chem. Soc.* **1992**, *114*, 7218.

(33) (a) Nesset, M. J. M. Ph.D. Thesis, University of Arizona, 1994. (b) Nesset, M. J. M.; Shokhireva, T. Kh.; Shokhirev, N. V.; Jacobson, S. E.; Walker, F. A. Manuscript in preparation.

(34) Miller, J. C.; Miller, J. N. *Statistics for Analytical Chemistry*, 3rd ed.; Ellis Horwood Prentice-Hall: New York, 1993.

(35) *Matlab*, version 4.1.1; The Mathworks, Inc.: Natick, MA, 1984−1993.

(36) (a) *Felix User Guide*, version 2.3; Biosym Technologies: San Diego, 1993. (b) *Felix Command Language Reference Guide*, version 2.3; Biosym Technologies: San Diego, CA, 1993.

(37) Güntert, P.; Wüthrich, K. *J. Magn. Reson.* **1992**, *96*, 403.

(38) Higgins, T. B., Safo, M. K., Scheidt, W. R. *Inorg. Chim. Acta* **1990**, *178*, 261.

(39) Ochsenbein, P.; Ayougou, K.; Mandon, D.; Fischer, J.; Weiss, R.; Austin, R. N.; Jayaraj, K.; Gold, A.; Terner, J.; Fajer, J. *Angew. Chem., Int. Ed. Engl.* **1994**, *33*, 348.

(40) (a) Mohamadi, F.; Richards, N. G. J.; Guida, W. C.; Liskamp, R.; Lipton, M.; Caufield, C.; Chang, G.; Hendrickson, T.; Still, W. K. *J. Comput. Chem.* **1990**, *11*, 440. (b) *MacroModel Interactive Molecular Modeling System*, version 4.5; MacroModel User Manual, Departmant of Chemistry, Columbia University: New York, 1994. (c) *MacroModel Interactive Molecular Modeling System*, version 4.5; BatchMin Reference Manual, Deptartment of Chemistry, Columbia University: New York, 1994.

(41) (a) *MacroModel Interactive Molecular Modeling System*, version 4.0; MacroModel User Manual, Department of Chemistry, Columbia University: New York, 1993. (b) *MacroModel Interactive Molecular Modeling System*, version 4.0; BatchMin Reference Manual, Department of Chemistry, Columbia University: New York, 1993.

(42) Korn, G. A.; Korn, T. M. *Mathematical Handbook for Scientists and Engineers*, 2nd ed.; McGraw-Hill: New York, 1968.

(43) *Sigma-Plot*, version 5.00; Jandel Scientific: Corte Madera, CA, 1986−1992.

(44) McQuarrie, D. A. *Statistical Thermodynamics;* University Science Books: Mill Valley, CA, 1993.

(45) Polam, J. R.; Shokhireva, T. Kh.; Raffii, K.; Simonis, U.; Walker, F. A. Submitted for publication in *Inorg. Chim. Acta*.